

Chapter 2

Ionization Front Physics

The early IGM was largely transparent to visible light due to the absence of dust and metals in primordial gas but was opaque to UV light with $\lambda \leq 912 \text{ \AA}$ because these photons can ionize hydrogen gas by the photoelectric effect. The hard UV luminosity of nascent massive primordial stars was not free to flow unimpeded into the universe but rather advanced by stages behind ionization fronts. For reasons detailed below the ionized gas was much hotter than its neutral environment, giving rise to astrophysical flows with important consequences for the evolution of the high-redshift universe. Hence, the study of early reionization is largely the study of the propagation of I-fronts into the IGM.

2.1 History

It was realized in the early 1900's that stars with surface temperatures above 20,000 K emit photons that could ionize hydrogen in their vicinity, and the resultant H II regions were observed in the 1930's. In 1939 Strömgren [43] performed the first analytical study of H II regions by considering the idealized problem of a point ionizing source of monochromatic photons switching on in a uniform infinite static hydrogen medium (one in which no fluid motions were permitted). He found that the outflow of UV photons from the central star ionizes a spherical zone which first expands but eventually halts. Since no gas motion occurs in this static model, the expansion is just the enlargement of the zone in which the interstellar medium (ISM) is ionized. Only 1 atom in 10^5 within the sphere remains neutral so the region is almost completely ionized. The outer boundary of the advancing (and then stationary) sphere is an abrupt transition from ionized to neutral hydrogen whose thickness is only a few UV photon mean free paths (mfp) through the neutral gas. In typical ISM densities the photon mfp is ~ 0.05 pc, which is short in comparison to the usual scales of astrophysical flows and the 10 - 20 pc diameters of common H II regions in the galaxy. The boundary can therefore be considered a discontinuity, which is why it was originally termed an ionization front. The distance at which the I-front halts is known as the Strömgren radius, and this marks the end of the *formation phase* of the H II region. In a static model the region can evolve no further.

Spitzer [44] and Kahn [45] continued this analysis by including ISM cooling and gas motion. Spitzer’s work on ISM cooling revealed that the excess kinetic energy inherited from UV photons by electrons would raise the temperature of the H II region to approximately 10^4 K. Kahn examined the evolution of ionization fronts in the context of the fluid equations and discovered several different classes of ionized flow in which shocks could emerge. He termed these fronts R-type and D-type, the nomenclature used today. Goldsworthy [46] and Axford [47] later studied in detail the character of the solutions to the fluid equations for ionization fronts, noting many parallels between supersonic R-type fronts and detonation waves and between D-type fronts and deflagration (or subsonic burn) fronts in combustion theory. Goldsworthy discovered similarity solutions for I-fronts in cylindrical and spherical symmetry in r^{-1} and $r^{-3/2}$ density gradients from the central source, respectively. Axford considered more general flows and numerically investigated the structure of the front itself and the transition of an R-type front to D-type.

Limited computational abilities confined the first numerical studies of H II regions in the 1960’s to 1D and fairly low resolutions [48, 49, 50]. However, these simulations confirmed what had earlier been predicted by the analytical work and are summarized in the review article by Mathews & O’Dell [51]. In particular, Mathews simulated the evolution of an R-type front but cut off the calculation immediately after it became D-type. Lasker followed the simulation of the front well beyond its conversion to D-

type. Both numerical and analytical studies continued through the late 1970's with 2D calculations, improved microphysics, and the investigation of fronts in stratified media. In particular, supersonic flows in H II regions were discovered in numerical simulations of ionization fronts blistering outward from the walls of molecular clouds ('champagne' flows). The data from one such simulation is shown in Fig 2.1. In the left panel the preferential flow of ionized matter down density gradients is evident in the longer velocity vectors directed outward through the center of the blister in the cloud wall. Work on the dynamics of H II regions in galactic environments through 1986 is comprehensively reviewed by Yorke [42].

A major advance in the 1990's was the theoretical analysis of ionization fronts emerging from radially symmetric power-law density gradients and isothermal self-gravitating disks by Franco *et al.* [41], which is discussed in detail below. Franco *et al.* implemented 1D semi-implicit lagrangian hydrocode simulations to validate their analytical results. In 1996 Garcia-Segura and Franco explored the breakup of dense shells in D-type fronts exhibiting initial density perturbations with 2D calculations [35]. The fragmentation of these shells into clumps was shown to be enhanced by the presence of the I-front at the inner wall of the shell. The growth of cometary tail-like instabilities in I-fronts sweeping through ambient inhomogeneities was studied numerically in 1998 by Mellema *et al.* , Canto *et al.* , and Soker [53, 54, 55], while theoretical and numerical analyses of shadowing instabilities in R-type fronts were performed in 2D planar geometry by Williams [56].

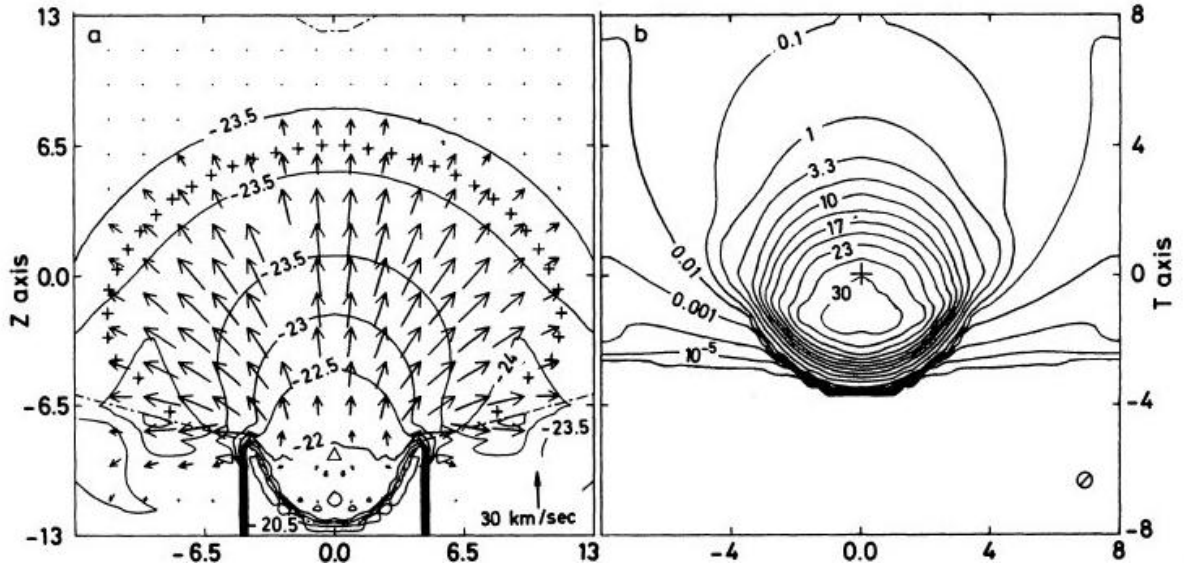


Figure 2.1: 2D numerical simulation of a the H II region of a massive O-type star born near the wall of a molecular hydrogen cloud core. Left panel: isodensity contour lines and fluid velocity vectors. Right panel: computed radio map of the H II region at $\lambda = 11$ cm. The ionization front 'blows out' the core wall, creating the blisterlike region shown. Ionized gas spills preferentially out through this exit in a champagne flow [52]. The flow is supersonic with respect to the ionized gas.

2D adaptive mesh radiation hydrodynamical calculations of the ionization of protostellar disks as their massive central stars emerge onto the main sequence were done by Yorke & Welz in 1996 [57] and are yet another example of the ubiquity of H II regions in stellar and galactic environments.

Numerical simulation of H II regions today falls into two classes: photoionization calculations and hydrodynamical evolution models. The goal of photoionization codes such as CLOUDY [58] is to incorporate the thousands of atomic transitions occurring in the metal ions of galactic nebulae to compile line emission profiles of these objects. Photoionization codes typically assume no gas motion (and are in fact often 1D) so they cannot be used to follow the dynamical evolution of the H II regions: all the effort is spent modeling the highly complex transition networks within them. In contrast, hydrocodes such as ZEUS-MP simulate the evolution of these structures over time. The ZEUS-MP calculations presented in Chapters 6 and 7 are the first 3D radiation hydrodynamical simulations of an H II region published to date.

2.2 Formation Phase in a Static Uniform Medium

At first, the ionization front recedes very quickly from the central star into the ISM. The velocity of the front is determined by the UV flux at the inner boundary that is capable of ionizing more neutral gas. If comoving with the front, one would see a neutral mass flux enter one side of the boundary and an ion flux exit the other side. This mass flux

is not arbitrary: only that flux can cross the boundary which can be ionized by the UV photons awaiting it on the other side. We can enforce this requirement with the following mass conservation jump condition across the discontinuous front:

$$\rho_i v_f = \overline{m}_i j_{ph} \quad (2.1)$$

where \overline{m}_i is the mean mass of the ions emerging from the other side of the boundary:

$$\overline{m}_i = \frac{n_H m_H + n_{He} m_{He}}{n_p + n_{He+}} \quad (2.2)$$

With number densities typical of molecular clouds and cosmic abundances of H and He, $\overline{m}_i = 1.40 m_H$ if He is not ionized and $1.27 m_H$ if it is. Given the photon output of an O-type star together with observed ISM densities one finds that ionization fronts initially recede from a star at several thousand kilometers per second.

2.2.1 The Strömgren Sphere

The number of neutrals permitted to cross the front per unit time (and hence the rate of advance v_f of the front) is controlled by the number of ionizing photons arriving at the inner boundary. These photons either reach the front directly from the central source or from recombinations to the ground state in the intervening ionized gas. Ground-state recombination photons add a diffuse component to the sphere's UV reservoir that does not have the r^{-2} falloff of the central flux. Because only 1 atom in 10^5 in the sphere remains neutral the diffuse photons can travel all the way to the front. However, these

recombination photons do not advance the front because the neutral atom they leave behind removes another source or diffuse photon that would otherwise have reached the front. Recombinations to any excited state of hydrogen (case B recombinations) yield one or more photons below the Lyman limit that exit the H II sphere because they are incapable of further ionization.

Two factors attenuate the number of photons reaching the I-front and slow it down. First, the expansion of the front geometrically dilutes the photons per unit area reaching the front by r^{-2} . Second, as the H II sphere grows the source photons encounter more neutrals from case B recombinations that do not replenish the UV supply needed to advance the front. The I-front slows as it expands, with its speed at any moment at any patch of the front being governed by the mass jump condition there. What eventually halts the front are case B recombinations: when the H II region becomes so large that the number of neutrals created within it by case B recombinations equals the number of photons emitted by the star per second, no source photons are left over to advance the front because the case B photons exit the sphere without further ionizations. The Strömgren radius can therefore be computed by equating the total number of source photons emitted per second to the number of case B recombinations occurring in the ionized sphere

$$\frac{4\pi}{3}R_S^3 n_e n_p \alpha_B = N_\nu \tag{2.3}$$

or

$$R_S = \left(\frac{3N_\nu}{4\pi\alpha_B n_H^2} \right)^{1/3} \quad (2.4)$$

where α_B is the recombination coefficient to $n=2$ and above. N_u is the total number of photons above the ionization limit leaving the surface of the star, R_S is the Strömgren radius, and n_e and n_p are the electron and proton number densities (which are essentially equal to the original H number density because it is completely ionized within the sphere). This derivation assumes uniform densities, an excellent approximation given that gas motion just begins to arise as the front reaches R_S .

2.2.2 Approach to the Strömgren Radius

Typical initial v_f 's for I-fronts are thousands of kilometers per second, much faster than the interstellar medium (ISM) sound speed (the rate at which disturbances can be acoustically communicated through the medium) so the ionized gas is essentially undisturbed by their passage. One can compute the approach of the I-front to the Strömgren radius as a function of time by applying eq (2.1) at the surface of the front. The rate of ionizing photons reaching the front equals the source photon rate minus the recombination rate to excited states in the volume bounded by the front, since each of these recombinations removes a source photon without re-emitting an ionizing photon. Recall that a recombination to the ground state also removes a source photon but releases another capable of advancing the front, with no net loss of ionizing UV—as if the removal of the source

photon never happened. Taking the ambient medium to be atomic hydrogen,

$$v_f = \frac{\bar{m}_i}{\rho_i} \dot{j}_{ph} = \frac{1}{n} \frac{n_{\gamma@front}}{4\pi r_f^2} = \frac{1}{n} \frac{1}{4\pi r_f^2} \left[N_\nu - \frac{4\pi}{3} r_f^3 n_e n_p \alpha_B \right] \quad (2.5)$$

Substituting eq (2.3) for N_ν and observing that $v_f = dr_f/dt$ yields

$$\frac{\frac{d}{dt}(r_f^3)}{r_s^3 - r_f^3} = n\alpha_B \quad (2.6)$$

Defining the variable $x = (r_f/r_s)^3$ and recognizing that at $t = 0$ $x = 0$, we can integrate both sides of the equation to obtain

$$\ln(1 - x) = n\alpha_B t \quad (2.7)$$

giving

$$r_f(t) = r_s \left(1 - e^{n\alpha_B t} \right)^{1/3} \quad (2.8)$$

The front at first moves quickly but soon slows, effectively reaching the Strömgren radius in 2 - 3 recombination times, as shown in Fig 2.2. This derivation ignores the temperature structure of the nebula in assuming α_B is constant but agrees with numerical studies incorporating these effects to within a few percent [59].

2.2.3 Ionization Profile of the Strömgren Sphere

In this section I review how Strömgren determined the neutral fraction of the equilibrium H II region to be uniformly 10^{-5} up to R_S , transitioning abruptly upward to 1 over a few UV photon mean free paths. Without presupposing a particular ionization profile as a

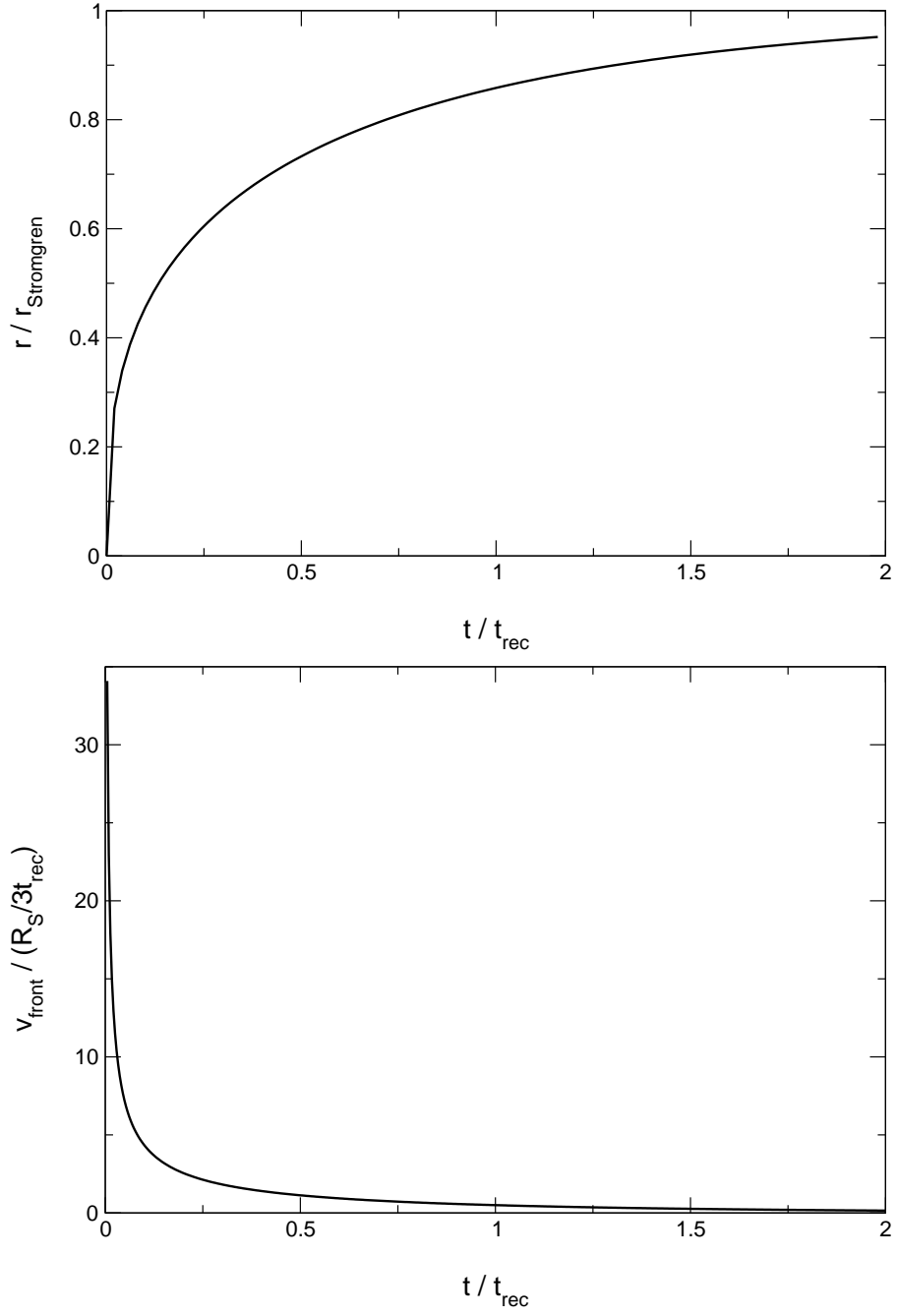


Figure 2.2: Time evolution of the radius and velocity of the ionization front in a static uniform medium. Upper panel: position of the front scaled by the Strömgren radius versus number of recombination times. Lower panel: velocity of the front scaled by $R_S/3t_{\text{rec}}$ versus number of recombination times.

function of radius, the interior of the H II region can be in equilibrium only if ionizations from the central source balance case B recombinations at all radii. Letting n , n_H , n_e , and n_p equal the total, neutral hydrogen, electron, and proton number densities respectively, we define the ionization fraction $x = n_e/n$. The neutral fraction is then $1-x$ and the equilibrium condition can be stated as

$$\int_{\nu_{th}}^{\infty} \sigma(1-x)n \frac{N_{\nu}}{4\pi r^2} e^{-(1-x)n\sigma r} d\nu = n^2 x^2 \alpha_B \quad (2.9)$$

The photoelectric cross section σ falls sharply with frequency ($\propto \nu^{-3}$) as does N_{ν} so the mean value theorem is often used to replace the integral with the integrand evaluated at the absorption edge of hydrogen:

$$\sigma_0(1-x)n \frac{N_{\nu}}{4\pi r^2} e^{-(1-x)n\sigma_0 r} = n^2 x^2 \alpha_B \quad (2.10)$$

$e^{-(1-x)n\sigma_0 r}$ encodes the removal of source photons en route to radius r by intervening neutral hydrogen; it is usually written as $e^{-\tau_{\nu}}$ with τ_{ν} defined to be the optical depth of the interior to ionizing UV:

$$\tau = (1-x)n\sigma_0 r \quad (2.11)$$

Since $1/n\sigma$ is the UV photon mean free path τ equals the number of mean free paths in the distance r . Then

$$d\tau = (1-x)n\sigma_0 dr \quad (2.12)$$

Dividing both sides of eq (2.10) by n^2 and $1-x$ and recognizing that $N_\nu/(4\pi r^2 n^2 \alpha_B) = \frac{1}{3}R_S^3$, eq (2.10) can be recast as

$$n\sigma_0 e^{-\tau} \frac{1}{r^2} \frac{1}{3} R_S^3 = \frac{x^2}{1-x} \quad (2.13)$$

Letting $y = e^{-\tau}$, $z = r^3/R_S^3$, and $\lambda = 1/n\sigma$ this equation reduces to

$$\frac{1-x}{x^2} = a \frac{1}{y} z^{2/3}, \quad a = \frac{3\lambda}{R_S} \quad (2.14)$$

Solving eq (2.12) for $1-x$ and substituting into eq (2.10) yields

$$\frac{dy}{dz} = -x^2 \quad (2.15)$$

with the same choice of new variables.

Equations (2.14) and (2.15) together define the ionization fraction as a function of radius for the Strömgren sphere. Given typical ISM parameters, $\lambda \sim 0.05$ pc and R_S is 10 - 20 pc, so the constant a is on the order of 0.001. By inspection, if y is close to 1 (small optical depth to photons at that radius) then $1-x \ll 1$ and the degree of ionization $x \approx 1$. This tells us that if photons can easily reach the radius r then the neutral fraction will be very low there, but not how x varies with r . The actual ionization profile can only be determined by numerical integration of eqs (2.14) and (2.15). Values of x^2 vs r/R_S for several choices of a are shown in the upper panel of Fig 2.3 (which is an actual image of Table 1 from Strömgren's 1939 seminal paper, included for historical interest). The ionization fraction abruptly drops over an interval of $0.004 R_S$ as r reaches R_S .

TABLE 1

x^2	s/s_0		
	$a=0.001$	$a=0.01$	$a=0.1$
1.0.....	0.000	0.000	0.00
0.8.....	1.000	0.988	0.82
0.6.....	1.002	1.009	0.97
0.4.....	1.003	1.020	1.05
0.2.....	1.004	1.028	1.12

TABLE 3

x^2	$z+\text{Constant}$ Normalized to 0 for $x^2=0.5$	x^2	$z+\text{Constant}$ Normalized to 0 for $x^2=0.5$
0.1.....	+5.3a	0.6.....	- 1.7a
.2.....	3.8	.7.....	4.2
.3.....	2.6	.8.....	8.6
.4.....	+1.3	0.9.....	-20.1
0.5.....	0.0		

Figure 2.3: Upper table: ionization fraction x as a function of r/R_S from the numerical integration of eqs (2.14) and (2.15). Lower table: change in x^2 with z in the thin neutral/ionized interface at the Strömberg radius. Both images are taken from Strömberg, 1939 [43].

One can better profile this jump in x^2 across the jump by setting $z = 1$ (or $r = R_S$) and directly integrating eqs (2.14) and (2.15) under the constraint that $y = 1$ when $z = 0$:

$$z = Const - a \left\{ \frac{1}{1-x} + 2 \ln \frac{x}{1-x} \right\} \quad (2.16)$$

This solution is a good approximation within the narrow transition; it is a family of identical curves offset by the constant of integration, which can be fixed by setting $z + \text{const} = 0$ when $x^2 = 0.25$. Strömgren's Table 3 of compiled x^2 values versus z is shown in the lower panel of Fig 2.3. Choosing $a \sim 0.001$ as before, the ionization fraction drops from 0.7 to 0.3 as z increases by 0.0053, corresponding to a fractional change in radius of ~ 0.002 , or several photon mean free paths in the neutral gas.

2.2.4 H II Region Cooling Processes

As noted earlier, since the front leaves the ionized gas undisturbed it is initially at the same density as when it was neutral. However, the gas is now much hotter than the ambient neutral medium because the photoelectrons acquire considerable kinetic energy from the UV photons and thermalize quickly through frequent collisions with the ions. Spitzer found that thermalization heats the ionized gas from the 10 - 100 K typical of molecular clouds in the galaxy today to 10^4 K [60]. In general, the final temperature to which the gas settles is controlled by the radiative processes that transport energy out of the Strömgren sphere. The complex network of cooling processes is usually summed

up in what is known as the ISM cooling curve, as illustrated in Fig 2.4.

Three processes dominate energy transport from H II regions in the galactic ISM [62]. At temperatures below 10^4 K collisional excitations of low-energy transitions in metals (note that astronomers term any element heavier than He a metal) dominate interstellar cooling rates. O^+ , O^{++} , and N^+ are common ions in modern H II regions (5 - 10 atoms per 10^5) which absorb kinetic energy through collisions with other atoms or free electrons and emit it as optical lines, giving rise to the spectacular displays of color in ionized nebulae in our galaxy. These transitions are known as *bound-bound* processes because the metallic species lose no electrons. The optical lines emitted by metals escape the I-sphere and cool it since they cannot excite hydrogen and are unlikely to encounter other metals in the ground state; even low concentrations of metals can be effective coolants. Optical cooling lines contribute the structure in the curve in Fig 2.4 below its upward jump at 10^4 K; this structure varies with the metallicity of the local ISM.

At 10^4 K both bound-bound and *bound-free* cooling is activated in hydrogen in the Strömgren sphere. Bound-bound processes occur because electrons, ions, and neutrals now can transfer sufficient kinetic energy to neutral hydrogen to stimulate line transitions below the Lyman limit that exit the H II region. Bound-free cooling begins as ionized hydrogen recombines to excited states, again emitting case B photons that exit the I-sphere. Recombinations dominate Strömgren sphere cooling because of its very low neutral fractions but both processes cool primordial minihalos with virial temperatures

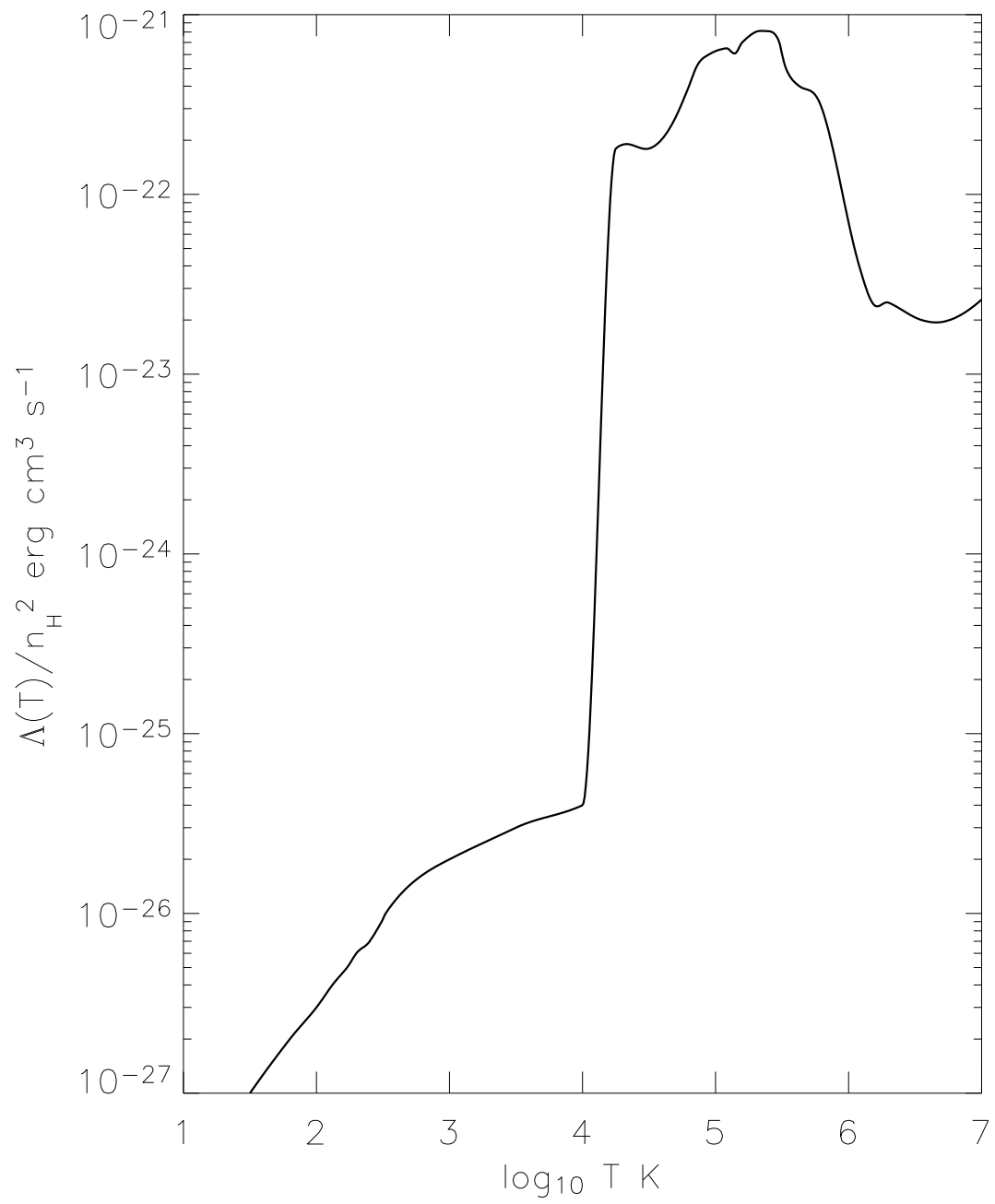


Figure 2.4: ISM cooling curve compiled by Dalgarno & McCray in 1972 [61]

above the threshold because collisional processes ionize or excite H at these temperatures even in the absence of ionizing UV.

One might think this cooling would return the mix to nearly its original temperature but recombinations preferentially remove the slower electrons and leave the hydrogen with a net energy gain. The cooling peaks just above 10^4 K and 10^5 K in the cooling curve are due to H and He recombinations, respectively. At progressively higher temperatures collisional excitation of metals continues but to more deeply-lying energy states. Above 10^6 K bremsstrahlung emission (a *free-free* process) dominates the ISM cooling curve. Though unimportant in 10^4 K H II regions, this process becomes prominent in the higher temperatures (10^6 K to 10^7 K) found in the highly shocked gas of wind bubbles.

The structure of the ISM cooling curve acts like a thermostat which sets galactic H II regions to temperatures of a few 10^4 K. When the ionized gas rises to 10^4 K the cooling rates jump four orders of magnitude and quench further photoionizational heating. Primordial cooling curves in ionized minihalos were simpler due to the absence of metals but still exhibited the H recombination jump that prevented early H II regions from rising above several 10^4 K. Pop III stars and quasars have harder UV spectra that deposit more energy per electron into H II regions and can ionize He but the He recombination cooling channel maintains the ionized gas below 10^5 K in these environments.

This analysis was performed under the assumption that photons are monochromatic at 13.6 eV H ionization energy. Two additional effects arise if one instead adopts a high

temperature blackbody or accretion spectrum as the radiation source; first, as mentioned above the H II region will be heated to higher temperatures (but still be regulated by He recombinational cooling). Second, the spectrum of photon energies will have a range of mean free paths, widening the sharp discontinuity of the front itself (with very hard spectra the width of the front can become the Hubble distance). Wide fronts can result in regions of the IGM being only partially ionized without accompanying large jumps in temperature. Catalysis by free electrons in the lower temperatures at the leading edge of broadened cosmological ionization fronts was the mechanism invoked by Ricotti *et al.* in 2001 for the rapid formation of H₂ in primordial H II regions.

Because the Strömgren sphere is 100 times hotter than its surrounding medium it has 200 times the pressure (since there are two ionized species for each neutral). A pressure wave develops in the ionized material which begins to push into the ambient ISM, and the H II region enters its *expansion phase*.

2.3 Dynamics of H II Regions in Uniform Media

Semi-analytical and numerical studies of the hydrodynamics of ionization fronts in uniform media have determined that ionized gas motion begins to affect the H II region just as the front reaches the Strömgren radius. The H II material begins to expand outward at roughly the speed of sound in the ionized gas. The sound speed governs how quickly disturbances in one region of the material can be communicated by acoustic (sonic) waves

to another region and is related to the pressure by

$$C_s = \sqrt{\frac{\gamma P}{\rho}} \quad (2.17)$$

Taking 1 and 2 as the neutral and ionized gas, respectively, $C_2 \sim 14 C_1$ because $P_2 \sim 200 P_1$ (for normal ISM parameters $C_1 \sim 1$ km/sec so $C_2 \sim 14$ km/sec). Because the ionized gas expands at a much higher speed than the sound speed of its neutral surroundings, the ambient gas cannot rearrange itself in time to move smoothly out of the way of the ionized flow. Neutral gas piles up just ahead of the front as the pressure wave steepens into a shock that is driven supersonically into the surrounding medium. The shock is an abrupt jump in gas velocity, density, and energy that arises from viscous processes in the flow. Its width is approximately the mean free path of an atom in the gas, which is so short in comparison to the dimensions of the flow features that it too can be treated as a mathematical discontinuity.

When the H II gas begins to inflate its density decreases, sharply reducing recombination rates in the gas because they are proportional to n^2 . Encountering fewer neutral atoms, more UV photons can now reach the ionization front (which slowed as it approached the Strömgren radius) and advance it forward. Hence, the front slows as it approaches R_S but does not stop as in the static case. The front continues to decelerate as it passes R_S because case B recombinations and geometry still attenuate the field, and at some point it slows to the sound speed of the ionized gas behind it. Any pressure perturbations in the hot ionized gas can now be sonically communicated to the front

itself, and it is roughly at this point that the building pressure wave in the expanding hot gas pushes past the front into the neutral upstream gas. If radiative cooling occurs in the shocked neutral gas, ambient material will accumulate onto it in a dense shell that is more difficult for the front to ionize, slowing it even further.

2.3.1 The Jump Conditions: Classes of I-Fronts

Kahn integrated Euler's equations of fluid dynamics across the sharp I-front discontinuity to discover what types of ionized flows would be possible. Assuming steady flow in the gas both upstream and downstream of the front, he derived the following jump conditions:

$$\rho_2 v_2 = \rho_1 v_1 \quad (= \overline{m}_i j_{ph}) \quad (2.18)$$

$$\rho_2 v_2^2 + P_2 = \rho_1 v_1^2 + P_1 \quad (2.19)$$

where ρ , v , and P are the gas density, velocity, and pressure in the reference frame comoving with the front, and the subscripts 1 and 2 again refer to the neutral and ionized gas. Steady upstream and downstream flow means that if one were comoving with the front upstream gas would approach at the constant speed v_1 and exit behind with speed v_2 , as illustrated in Fig 2.5. Steady flow is valid if a parcel of gas in the front is ionized on timescales that are short in comparison to changes in the flow itself and allows one to drop the partial time derivatives in the integration of Euler's equations across the discontinuity. This condition can be violated if the front encounters dense clumps, as discussed in Chapter 6.

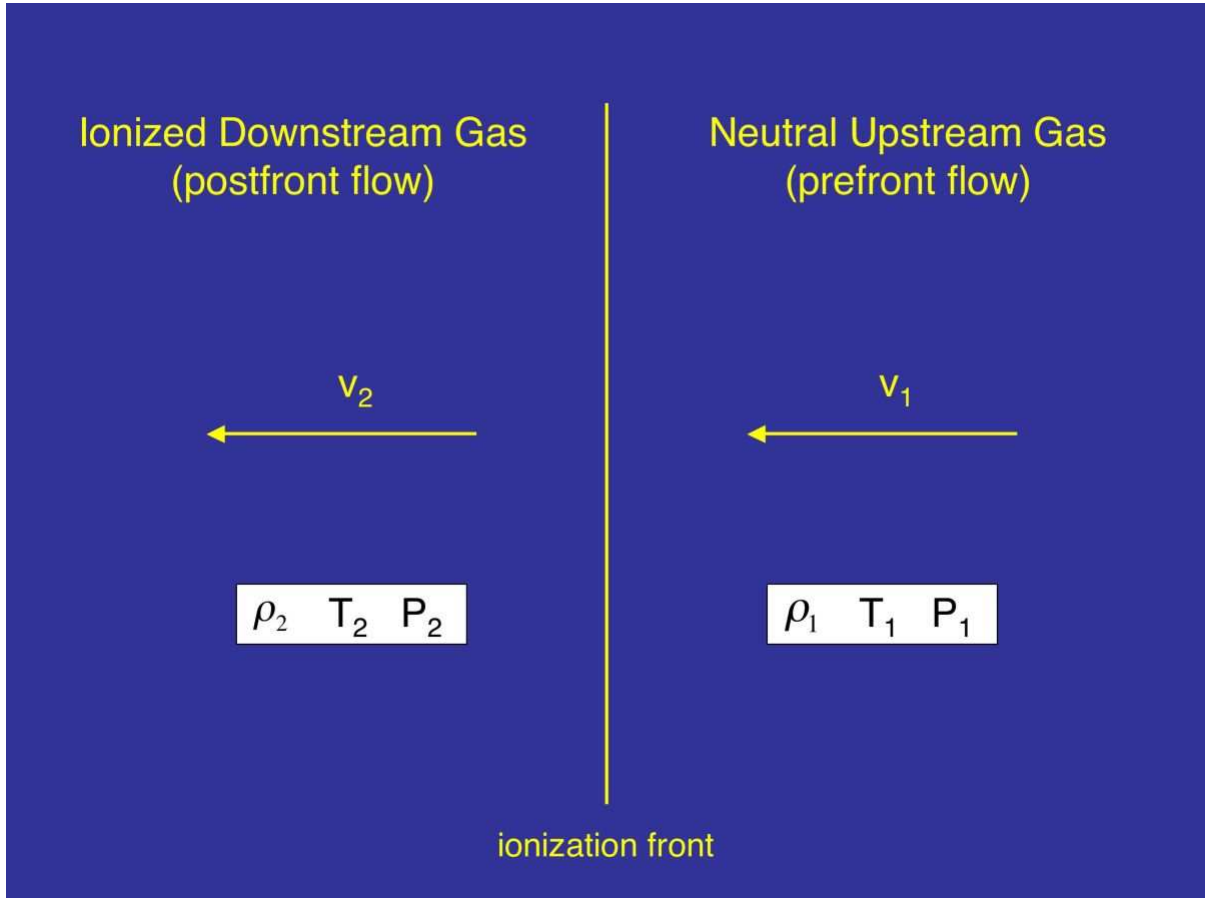


Figure 2.5: Jump in steady-flow fluid variables across an ionization front, as seen by an observer in the frame of the front (which moves to the right in the laboratory frame in this diagram). Region 1 is the neutral ambient medium and region 2 is the ionized postfront gas.

P can be eliminated in favor of C, the isothermal sound speed, in eq (2.19):

$$\rho_2(v_2^2 + C_2^2) = \rho_1(v_1^2 + C_1^2) \quad (2.20)$$

Solving for v_2 , one finds

$$v_2^2 - \left(v_1 + \frac{C_1^2}{v_1} \right) v_2 + C_2^2 = 0 \quad (2.21)$$

for which real solutions exist only if

$$v_1 + \frac{C_1^2}{v_1} > 2C_2 \quad (2.22)$$

or

$$v_1^2 - 2C_2v_1 + C_1^2 = f(v_1) > 0 \quad (2.23)$$

$f(v_1)$ is a parabola in the v_1 - f plane with two roots:

$$v_D = C_2 - (C_2^2 - C_1^2)^{1/2} \simeq \frac{C_1^2}{2C_2} \quad (2.24)$$

and

$$v_R = C_2 + (C_2^2 - C_1^2)^{1/2} \simeq 2C_2 \quad (2.25)$$

$f(v_1) < 0$ for $v_D < v_1 < v_R$ so real values of v_2 are only possible if $v_1 (= v_{front}) > v_R$ or $v_1 < v_D$. If $v_1 > v_R$ the front is said to be R-type. Historically, this name followed from the fact that if ρ_1 is small (a *R*arified medium) then v_1 is large from eq (2.18) and the front moves rapidly through the ISM. In contrast, if $v_1 < v_D$ the front is said to be D-type: if ρ_1 is large (a *D*ense medium) then the front moves slowly relative to the

neutral medium it encounters. If $v_f = v_R$ the front is *R-critical* and if $v_f = v_D$ the front is *D-critical*.

Equations (2.24) and (2.25) imply that R-type fronts move supersonically with respect to the neutral prefront material while D-type fronts propagate subsonically since $v_R > C_1$ but $v_D < C_1$. For either choice of v_1 the jump conditions permit two possibilities for v_2 , which can be derived from eq (2.21) by noting that the product of the two roots of the quadratic equation is equal to its constant term:

$$v_2^{(1)}v_2^{(2)} = C_2^2 \quad (2.26)$$

Assuming that the solutions are distinct, eq (2.26) implies that the ionized gas moves either supersonically ($v_2 > C_2$) or subsonically ($v_2 < C_2$) with respect to the front. The ratio of the postfront and neutral densities can also be derived from eq (2.21):

$$\frac{\rho_2}{\rho_1} = \frac{v_1}{v_2} \text{ (from eq (2.18))} = \frac{(v_1^2 + C_1^2) \mp [(v_1^2 + C_1^2)^2 - 4v_1^2C_2^2]^{1/2}}{2C_2^2} \quad (2.27)$$

Both R-type and D-type fronts are further classified according to this ratio: if $\rho_2/\rho_1 \simeq 1$ the front is referred to as *weak*. If ρ_2/ρ_1 is \gg or $\ll 1$ then it is referred to as *strong*.

Weak R-type Fronts

It can be shown from eq (2.27) for an R-type front that if $v_2 > C_2$ then $\rho_2/\rho_1 \simeq 1$ and it is weak R-type. If the front is highly supersonic through the neutral gas then $v_1 \gg$

v_R and it can be shown from binomial expansion of eq (2.27) that

$$\frac{\rho_2}{\rho_1} \simeq 1 + \frac{C_2^2}{v_1^2} \quad (2.28)$$

$v_1 \geq 2C_2$ so $1 \geq \rho_2/\rho_1 \geq 5/4$. There is little or no density jump because the ionization front moves too quickly for the medium to hydrodynamically respond. Supersonic upstream and downstream velocities in the frame of the front translate into supersonic front speeds and negligible ionized gas motion in the lab frame. In the moving frame upstream gas would appear to flow virtually unimpeded through the I-front and quickly exit as ionized gas. Nascent ionization fronts of zero-age main sequence (ZAMS) massive stars are weak R-type.

Strong R-type Fronts

If $v_2 < C_2$ for the R-type front then it follows from eq (2.27) that $\rho_2/\rho_1 > 1$ and the ionized gas is denser than the ambient gas; this is an example of a strong R-type front. A subsonic v_2 in the moving frame implies that the ionized gas is strongly accelerated forward behind the front in the lab frame. No known mechanism in the ISM can accelerate hot dense gas behind the front in this manner based on photoionization alone, so strong R-type fronts are not thought to exist in nature. Osterbrock [62] also notes that the subsonic v_2 would allow any disturbances in the postfront gas to be constantly communicated to the front, thereby disrupting or weakening it.

Strong D-type Fronts

If $v_2 > C_2$ for a D-type front then eq (2.27) predicts that $\rho_2/\rho_1 \gg 1$ and the neutral medium just ahead of the front must be much denser than the ionized gas: a strong D-type front. This solution cannot describe the evolution of an H II region around a star centered in a molecular cloud core because in the frame of the front the ionized gas rushes supersonically back toward the star. Since the front itself only advances subsonically away from the star the ionized gas would concentrate at the star itself, unable to provide the pressure support that drives the front. However, ionized supersonic backflows and strong D-type fronts may arise when a massive star external to a cloud photoionizes it. In this scenario the ionization front slowly evaporates the outer layers of the star, which are expelled backward by steep density gradients in the ionized isothermal gas.

Weak D-type Fronts

If $v_2 < C_2$ then $\rho_1/\rho_2 \simeq 1$ and the front is weak D-type; however, this statement must be qualified. Binomial expansion of eq (2.27) under these circumstances gives

$$\frac{C_1^2}{2C_2^2} \leq \frac{\rho_2}{\rho_1} \leq \frac{C_1^2}{C_2^2} \quad (2.29)$$

Consider the density, velocity, and temperature profiles of the ionization front shown in Fig 2.6. The drop in temperature from 20,000 K ionized gas to 1200 K shocked gas marks the position of the I-front. Even though the front moves supersonically at 7.5 km/sec with respect to the undisturbed neutral medium (whose sound speed is only 1 km/sec)

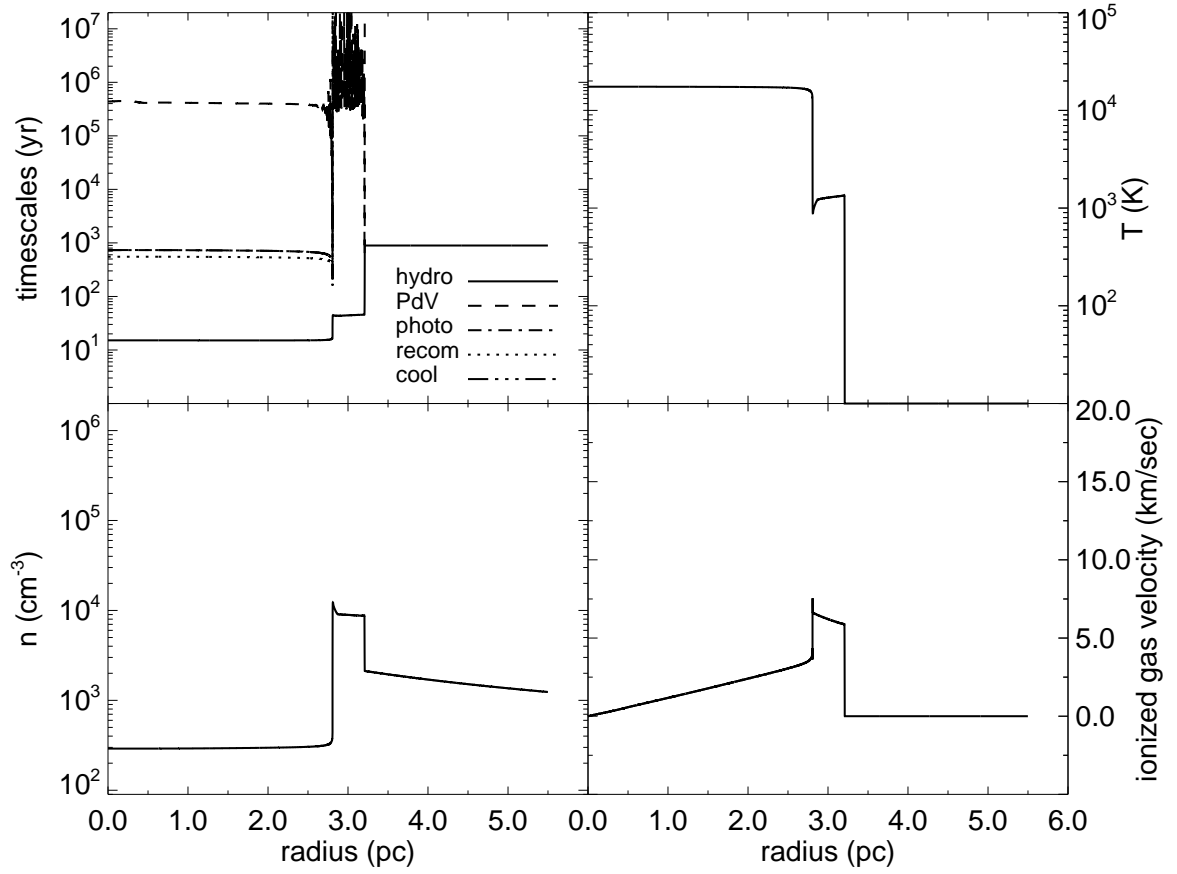


Figure 2.6: ZEUS-MP simulation of a D-type ionization front due to a small OB association of stars centered in a flat central density core of radius 2.1×10^{16} cm and $n = 10^6 \text{ cm}^{-3}$. The core is surrounded by an r^{-1} envelope and the central photon emission rate is $5.0 \times 10^{49} \text{ s}^{-1}$ with mean energy $h\nu = 17.0 \text{ eV}$. The hydrodynamical and timescale profiles are taken at $3.28 \times 10^5 \text{ yr}$.

it is D-type. The upstream gas the front actually encounters is shocked neutral gas also moving outward at nearly the same speed so their relative velocity is much lower than C_1 . The density jump at the I-front $\rho_2/\rho_1 \sim 300/10^4$ or $1/30$. Given the large departure of this ratio from 1 it might be thought that the front is strong D-type. However, the velocity profile shows the ionized backflow to be subsonic with respect to its own 16 km/sec sound speed, in apparent contradiction to the strong-D criterion. The flat densities behind the front are additional evidence of subsonic flow: as noted earlier, in these circumstances pressure fluctuations arising from density perturbations in the isothermal postfront gas propagate as acoustic waves that reach the I-front and smoothen the features.

Applying the sound speeds in this simulation to eq (2.29) (remembering that $C_s \propto T^{1/2}$) we find that

$$\frac{C_1^2}{2C_2^2} \sim 1200/40000 \leq \frac{\rho_2}{\rho_1} = 1/30 \leq 1200/20000 = \frac{C_1^2}{C_2^2} \quad (2.30)$$

so the jump conditions for a weak D-type front are satisfied, in spite of the large ratio in densities. Eq (2.29) encompasses larger density ratios than are implied by the common stipulation that ρ_1/ρ_2 must be approximately 1 for weak D-type fronts. Nonetheless, these ratios are still close to one in comparison to those of strong D-type fronts. Weak D-type solutions describe the propagation of hydrodynamical ionization fronts from stars deeply imbedded in cloud cores with densities that are either constant or fall off gently with radius.

The I-front jump conditions only dictate what combinations of densities and velocities are permissible on either side of the discontinuity, not what ionized hydrodynamics will actually arise in a given scenario. The jump conditions can accomodate a variety of astrophysical flows such as shocks and rarefaction waves; conversely, ionized flows readjust themselves to satisfy the conservation equations across the I-front. To fully understand the dynamical evolution of any ionization front one must coevolve the equations of fluid dynamics, ionization, and radiative transfer together for the conditions at hand.

2.3.2 Expansion Phase of the H II Region

In 1961 Axford [47] and Goldsworthy [46] performed such an analysis by numerically advancing the fluid and ionization equations in time for a variety of I-fronts. The simple physical reasoning outlined at the beginning of this section was confirmed in their studies: when a star turns on in a uniform medium an ionization front that is initially weak R-type flashes away from it into the ISM. It becomes R-critical when it slows to approximately $2C_2$ near the Strömgren radius. The front then descends the forbidden velocity range predicted by Khan and becomes D-critical at $v_f = v_D$.

When the front slows to C_2 the pressure wave building behind the front detaches from it as a shock into the neutral material. The shock, driven by the ram pressure of the ionized gas behind it, accumulates neutral gas in a dense shell when radiative processes from the shock are taken into account. Axford succeeded in numerically resolving both

the ionization structure of the thin front as well as the formation and advance of the shock through it. Earlier both the front and the shock were treated as discontinuities but in reality the shock is much thinner than the front because atoms have a much smaller mean free path through the gas than do UV photons. At typical ISM densities the front is 10 to 20 times wider than the shock. Axford found that the ionization fraction decreased exponentially across the thin ionization layer.

It is sometimes thought that the front abruptly downshifts across the forbidden velocity range and trades places with the shock but Axford found that it eases through a sequence of quasi-steady states to become D-type. The transition begins when the front decelerates to the adiabatic sound speed of the ionized gas, becoming sonically connected to it. The pressure wave that has been building behind the front steepens into a weak shock *within* the I-front discontinuity for typical ISM cooling laws and incident UV fluxes. As the thin front continues to slow due to r^{-2} falloff of central flux and recombinations, the weak shock advances through it and strengthens. It emerges and becomes distinct from the front when it has swept up a column density of neutral gas equal to the photoionization cross section of the UV photons. Interestingly, Axford discovered cases in which 0, 1, and even 2 shocks formed inside the front discontinuity. The ionization front is neither strictly R-type nor D-type during its exchange with the shock because it departs from steady flow.

Now weak D-type, the front evolves according to the approximate result [60]

$$r_i(t) = R_S \left(1 + \frac{4}{7} \frac{c_{II} t}{R_S} \right)^{\frac{4}{7}} \quad (2.31)$$

so long as $P_i \gg P_0$, the pressure of the ambient medium (R_S is the Strömgren radius of the static solution). Expansion continues but slows (as seen in the derivative of $r_i(t)$ above) until the H II region comes to pressure equilibrium with its environment. The evolution of the ionization front is thus

$$weak - R \longrightarrow R - critical \longrightarrow D - critical \longrightarrow weak - D \quad (2.32)$$

2.3.3 Approach to Pressure Equilibrium

The internal pressure of the H II region drops as it expands even though new material is ionized. Recalling that two ions are created per neutral atom

$$P_i = 2n_i k_B T_i \quad (2.33)$$

where n_i and T_i are electron density and temperature. The average ion density in the H II region decreases by expansion but increases as the front ionizes more neutrals. It is ultimately determined by the case B recombinations within the region. The relatively slow D-type front expands through a succession of states in which central photon emission is nearly balanced by case B recombinations, as in the determination of the initial Strömgren radius. It is the small departures from this equilibrium that move the front forward. To compute the ion density in the H II region, to first order it is assumed that

source photons balance case B recombinations:

$$\langle n_i \rangle \simeq \left(\frac{3N_\nu}{4\pi\alpha_B} \right)^{1/2} R_f^{-3/2} \quad (2.34)$$

$\langle n_i \rangle$ is a volume averaged ion density but is fairly close to the local density at any point in the region after the expansion of the front becomes subsonic with respect to the ionized gas. ISM cooling keeps the gas isothermal, so any density variations again give rise to pressure fluctuations creating acoustic waves that smoothen the density ripples: n_i is nearly uniform with radius, as discussed earlier. Since $R_f \propto t^{4/7}$ the pressure in the H II region evolves as $t^{-6/7}$ as long as $P_i \gg P_0$, the pressure in the neutral ambient gas.

As the internal pressure falls the shock weakens. When the H II region halts it must be a new Strömgren sphere in pressure equilibrium with its environment:

$$R_{final} = \left(\frac{3N_\nu}{4\pi\alpha_B n_f^2} \right)^{1/3} \quad (2.35)$$

R_{final} can be expressed in terms of the original Strömgren radius R_S by dividing this equation by eq (2.4)

$$\frac{R_{final}}{R_S} = \left(\frac{n_0}{n_{final}} \right)^{2/3} \quad (2.36)$$

where n_{final} is the final ion density in the H II region and n_0 is the ion density in the original Strömgren sphere. n_0 is equal to the ambient number density because the initial Strömgren sphere was formed before the ionized gas became dynamic. Final pressure equilibrium implies that

$$2n_{final}k_B T_i = n_0 k_B T_0 \quad (2.37)$$

so

$$R_{final} = R_S \left(\frac{2T_i}{T_0} \right)^{2/3} \quad (2.38)$$

For O-type stars in the galaxy $R_{final} \sim 60 R_S$. At the densities of many molecular hydrogen cloud cores the star exits the main sequence before the H II region can achieve pressure equilibrium. However, molecular cores with central densities $\sim 10^7 \text{ cm}^{-3}$ and warm (100 K) temperatures have recently been observed [63] with higher pressures that can quickly confine the I-front to a stable compact long-lived structure known as an ultracompact H II (UCH II) region. Because these dense cores are self-gravitating, large thermal pressures support them against collapse; it is the large downward pressure from the material in the upper layers of the core that halt the emergent front. As illustrated in Fig 2.7, UCH II regions range from 0.01 pc to 0.1 pc in size and were initially believed to be the early stages of expanding H II regions surrounding newborn massive stars. This led to what is known as the UCH II lifetime problem in the late 1980's [65] because 10 times more of these objects were observed in the galaxy than was consistent with known star formation rates. The dilemma is resolved if these structures are actually persistent non-dynamical objects so pressure confinement of I-fronts has been cited as a possible solution to the lifetime problem [35].

Numerical simulations by Garcia-Segura and Franco [35] indicate that the shock reverts to a pressure wave as the ionization front halts. The wave propagates outward as an acoustic wave that is eventually damped by the viscosity of the gas in the molecular

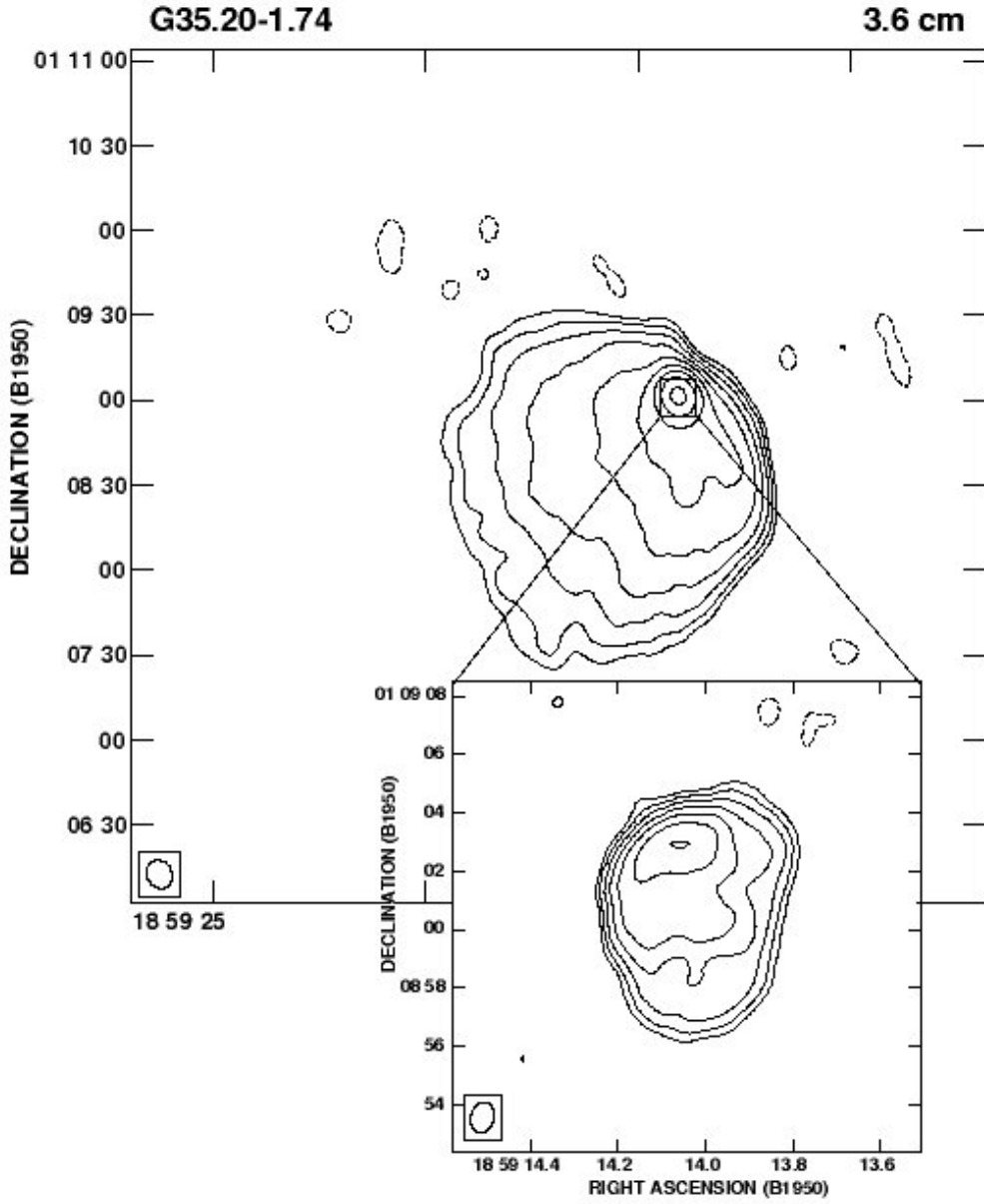


Figure 2.7: Galactic UCH II region radio image. Taken from a high-resolution VLA survey [64], the larger image has an angular diameter of 2 arcminutes (corresponding to size of 1.9 pc) and maps the extended radio emission from its ultracompact central H II source. The central source shown in the inset has an angular diameter of 6 arcseconds, or 0.1 pc.

core.

2.4 I-fronts in Power-Law Densities

Uniform media are a simplified ideal of the power-law or disk-type densities that shroud young hot stars in the galaxy today. Recent radio observations of cloud fragments and isolated dark clouds have revealed internal power-law density distributions r^{-w} with w ranging from 1 to 3 and with $w \sim 2$ as an average [66]. Visual extinction studies of nearby northern and southern clouds have corroborated these gradients [67]. High-resolution radio observations of star-forming regions have also uncovered dense elongated structures surrounding newborn stars that are suggestive of protostellar disks. Protostars are often located in circumstellar disks opaque to visible wavelengths but not to infrared. IR data taken of young stellar objects have features attributable to dusty circumstellar disks [68, 69]. The highest resolution simulations of primordial Pop III star formation to date with elements as small as $\sim 100 R_{\odot}$ and $\sim 1/4 M_{\odot}$ [3] indicate that the first stars resided in clouds that are roughly spherical on scales from ~ 0.1 pc out to the virial radii (~ 100 pc), with masses of approximately $100 M_{\odot}$ accreting within dark matter halos on the order of $10^6 M_{\odot}$ and forming by redshifts of 20 - 30. Hence, primordial fronts ionizing high-redshift halos likely exhibited many of the same features found the present-day I-fronts in H II regions.

The galactic observations cited above motivated Franco *et al.* [41] to perform analyt-

ical studies of 1-D ionization fronts from a monochromatic source of photons centered in a radial density profile with a flat central core followed by an $r^{-\omega}$ dropoff:

$$n_H(r) = \begin{cases} n_c & \text{if } r \leq r_c \\ n_c(r/r_c)^{-\omega} & \text{if } r \geq r_c \end{cases}$$

They considered photon rates whose Strömgren radius R_S in an infinite medium of density n_c was greater than r_c and thus in the gradient, noting that if $R_S < r_c$ the front would evolve as if in a constant density. Their analysis of I-front propagation down the radial density falloff revealed that there is a critical exponent

$$\omega_{crit} = \frac{3}{2} \left[1 - \left(\frac{r_c}{R_S} \right)^3 \right]^{-1} \quad (2.39)$$

below which the front executes the classic approach to a Strömgren sphere of modified radius

$$R_\omega = R_S \left[\frac{3-2\omega}{3} + \frac{2\omega}{3} \left(\frac{r_c}{R_S} \right)^3 \right]^{1/(3-2\omega)} \left(\frac{R_S}{r_c} \right)^{2\omega/(3-2\omega)} \quad (2.40)$$

reverts from R-type to D-type, and continues along the gradient, building up a dense shocked shell before it. Here R_S is the classical Strömgren radius the ionization front would have in a uniform density medium n_c :

$$R_S = \left(\frac{3\dot{n}_{ph}}{4\pi\alpha_B n_c^2} \right)^{1/3} \quad (2.41)$$

If $\omega < 1.5 < \omega_{crit}$ the front remains D-type throughout its lifetime and continues to accumulate mass in its shell, evolving as

$$R(t) = R_\omega \left[1 + \frac{7 - 2\omega}{4} + \left(\frac{12}{9 - 4\omega} \right)^{1/2} \frac{c_i t}{R_\omega} \right]^{4/(7-2\omega)} \quad (2.42)$$

where c_i is the sound speed in the ionized gas. If $\omega = 1.5$ the shock and front coincide without any formation of a thin neutral shell as in the $\omega < 1.5$ profiles. When $1.5 < \omega < \omega_{crit}$ the D-type front will revert back to R-type and quickly overrun the entire cloud. Since I-fronts ultimately transform back to R-type in any cloud with density dropoffs steeper than 1.5 this power constitutes the critical point for eventual runaway ionization. As expected, if $\omega = 0$ then R_ω becomes R_S and $R(t)$ exhibits the $t^{4/7}$ expansion of an ionization front in a uniform medium.

Fronts descending gradients steeper than $r^{-\omega_{crit}}$ never slow to a Strömgren radius or transform to D-type. Remaining R-type, they quickly ionize the entire cloud, leaving behind an essentially undisturbed ionized density profile because they exit on timescales that are short in comparison to any hydrodynamical response of the gas. Completely ionized and at much higher pressures, the entire cloud begins to inflate outward at the sound speed of the ionized material. However, the abrupt core density dropoff left undisturbed by the rapid exit of the front develops a large pressure gradient because of the equation of state in the nearly isothermal postfront gas

$$P \propto E = c_{iso}^2 \rho \quad (2.43)$$

The sharpest pressure gradient is at the ionized core's edge at $r \sim r_c$. This edge expands outward in a pressure wave which quickly becomes a shock that overtakes the more slowly

moving outer cloud regions. The velocity of this shock depends on the steepness of the density dropoff beyond the core: if $\omega_{crit} < \omega < 3$ then

$$r_c(t) \simeq r_c + \left[1 + \left(\frac{3}{3 - \omega} \right)^{1/2} \right] c_i t \quad (2.44)$$

If $\omega = 3$ then

$$r_c(t) \simeq 3.2 r_c \left(\frac{c_i t}{r_c} \right)^{1.1} \quad (2.45)$$

and if $\omega > 3$

$$r_c(t) \simeq r_c \left[1 + \left(\frac{4}{\omega - 3} \right)^{1/2} \left(\frac{\delta + 2 - \omega}{2} \right) \left(\frac{c_i t}{r_c} \right) \right]^{2/(\delta + 2 - \omega)} \quad (2.46)$$

where r_c is the initial core radius and δ is an empirically fit function of ω :

$$\delta \simeq 0.55 (\omega - 3) + 2.8 \quad (2.47)$$

The shock has a constant velocity for $\omega_{crit} < \omega \leq 3$, weakly accelerates for $\omega = 3$, and strongly accelerates if $\omega > 3$. This is in agreement with what would be expected for the mass of each cloud. For $\omega < 3$ the cloud mass is infinite so a central energy source could not produce gas velocities that increase with time. The cloud mass becomes finite just above $\omega = 3$, the threshold for the ionized flow to exhibit a positive acceleration.

I present detailed time-dependent hydrodynamical profiles as well as process timescale plots in Chapter 4 that shed further light on the microphysics governing the gas dynamics of ionization fronts and flows in the stratified envelopes surrounding luminous UV

sources. The I-front evolution outlined in this chapter pertains to uniform or radially symmetric media, but new hydrodynamical phenomena arise when I-fronts encounter inhomogeneities in three-dimensional environments. Recent theoretical and numerical analyses have found that both R-type and D-type ionization fronts can develop dynamical instabilities manifest as ionized fingers and jets that extend into the neutral material in advance of the front. These features can clump neutral gas into overdensities of 10^3 to 10^4 along adjacent lines of sight that accrue tens of solar masses of material, with potentially important consequences for star formation. I defer discussion of these phenomena to Chapter 6, where I describe the 3D trials of our ZEUS-MP code.